Eur. Phys. J. A (2020) 56:223
https://doi.org/10.1140/epja/s10050-020-00232-7

THE EUROPEAN PHYSICAL JOURNAL A

Review

Hadron production in elementary nucleon–nucleon reactions from low to ultra-relativistic energies

V. Kireyeu[1], I. Grishmanovskii[2], V. Kolesnikov[1], V. Voronyuk[1], E. Bratkovskaya[2,3,a]

[1] Joint Institute for Nuclear Research, Joliot-Curie 6, 141980 Dubna, Moscow Region, Russia
[2] Institute for Theoretical Physics, Johann Wolfgang Goethe Universität, Frankfurt am Main, Germany
[3] GSI Helmholtzzentrum für Schwerionenforschung GmbH, Planckstrasse 1, 64291 Darmstadt, Germany

Received: 25 June 2020 / Accepted: 23 August 2020 / Published online: 4 September 2020

Communicated by Laura Tolos

Abstract We study the hadron production in $p+p$, $p+n$ and $n+n$ reactions within the microscopic Parton–Hadron-Dynamics (PHSD) transport approach in comparison to PYTHIA 8.2. We discuss the details of the "PHSD tune" of the Lund string model (realized by event generators FRITIOF and PYTHIA) in the vacuum (as in $N+N$ collisions) as well as its in-medium modifications relevant for heavy-ion collisions where a hot and dense matter is produced. We compare the results of PHSD and PYTHIA 8.2 (default version) for the excitation function of hadron multiplicities as well as differential rapidity y, transverse momentum p_T and x_F distributions in $p+p$, $p+n$ and $n+n$ reactions with the existing experimental data in the energy range $\sqrt{s_{NN}} = 2.7-7000$ GeV. We discuss the production mechanisms of hadrons and the role of final state interactions (FSI) due to the hadronic rescattering. We also show the influence of the possible quark–gluon plasma (QGP) formation on hadronic observables in $p+p$ collisions at LHC energies. We stress the importance of developing a reliable event generator for elementary reactions from low to ultra-relativistic energies in view of actual and upcoming heavy-ion experiments.

1 Introduction

An understanding of the mechanisms of multiparticle production in elementary nucleon–nucleon (NN) collisions in a wide energy range – from a few GeV up to a few TeV – is one of the challenging topics in hadron physics. This has a high impact on heavy-ion physics as well since in heavy-ion collisions (HIC) one probes the matter created by many individual NN scatterings – from primary highly energetic NN scattering during the initial phase of overlapping nuclei up to secondary low energy NN collisions occurring during the final state interactions (FSI) of the expanding system. Thus, for the description of the HIC one needs to know the elementary hadron-hadron (hh) collisions: baryon–baryon (BB), meson–baryon (mB) and meson–meson (mm) collisions, in particular for hadron multiplicities, i.e. flavour 'chemistry', as well as their momentum distributions. Moreover, the elementary NN reactions are used in HICs as a "reference frame" to study many physical effects related to the properties of the hot and dense matter created in HICs. For example, the most common way to present HIC results for hard probes (i = charm or jets), is to show the ratio of their production probability in $A+A$ collisions relative to $p+p$ collisions scaled with the number of binary collisions N_{bin}: $R^i_{AA} = \sigma^i_{AA}/(\sigma^i_{pp} \cdot N_{bin})$. The deviation of the ratio from unity provides information on the in-medium effects.

One of the most successful and commonly used models for the description of elementary collisions from the GeV to the TeV energy range is the Lund string model [1,2] which describes the energetic hadron–hadron collisions by the creation of excited color-singlet states, denoted by "strings", which are realized within the FRITIOF [3,4] and PYTHIA models [5] in terms of particle event generators. A string is composed of two string ends corresponding to the leading constituent quarks (antiquarks) of the colliding hadrons and a color flux tube (color-electric field) in between. As the string ends recede, virtual $q\bar{q}$ or $qq\bar{q}\bar{q}$ pairs are produced in the uniform color field by a tunneling process (described by the Schwinger formula [6]), causing the breaking of the string and producing new matter from field energy.

The Lund model is extremely successful in describing a huge variety of observables at high energies. The event generator PYTHIA is very often used by experimental collaborations for a comparison with the measured data as well as for simulations of the detector set up. The Lund

[a] e-mail: Elena.Bratkovskaya@th.physik.uni-frankfurt.de (corresponding author)

model is employed in heavy-ion transport approaches for the simulation of multiparticle production in elementary hadron-hadron collisions which happened during the time evolution of relativistic heavy-ion reactions. The FRITIOF and PYTHIA event generators are incorporated in the off-shell Parton–Hadron-String Dynamics approach (PHSD) [7–11] and it's early version Hadron-String Dynamics (HSD) [12] (cf. the HSD review [12] for the description of string dynamics in HICs) as well as in the recent extension of the PHSD for the cluster formation, the Parton–Hadron–Quantum-Molecular Dynamics (PHQMD) [13] based on the quantum-molecular dynamics (QMD) propagation of hadrons. Moreover, PYTHIA is used in UrQMD [14,15], GiBUU [16], SMASH [17] etc. We note that there are alternative event generators for hadron–hadron collisions such as EPOS [18,19], QGSJET [20], HERWIG [21] etc.

Most hadron–hadron event generators have been constructed for the description of ultra-relativistic $p + p$ collisions or cosmic rays at very high energies. However, the use of hh event generators in the transport approaches for HICs has a very important specification: as mentioned above, the energy range of hh reactions – taking place during the HIC evolution – is very wide, e.g. even if one considers $A + A$ collisions at LHC energies, the secondary reactions, which take place after the hadronization of the quark–gluon plasma created in such HIC collisions, cover a very broad interval of the invariant energy $\sqrt{s}$. Thus, the hh generator must have a wide range of applicability, i.e. from a few GeV to a few TeV. In this respect the Lund event generators (FRITIOF and PYTHIA) are quite suitable and provide a rather convincing description of inelastic hh collisions from high energies to the lower ones. However, some improvement of the model, i.e. "tuning", is required for an extension to low energies: adjustment of the flavour chemistry of the produced particles and their distributions. Moreover, in HICs the string fragments in the hot and dense environment which might lead to a modification of the fragmentation mechanism and the properties of the produced hadrons. Such modifications have been incorporated in the FRITIOF 7.02 and PYTHIA 6.4 models during the development of the PHSD(HSD) approach which we will call as "PHSD tune".

In this study we perform a systematic analysis of the the hadron production in $p+p$, $p+n$ and $n+n$ reactions within the microscopic PHSD transport approach and PYTHIA 8.2 in its default version. We present the details of the "PHSD tune" of the Lund generators FRITIOF 7.02 and PYTHIA 6.4 for the inelastic hh collisions in the vacuum. Furthermore, we discuss the in-medium extension of the Lund string model for heavy-ion collisions where the string formation and decay occurs in a hot and dense environment. We provide a detailed comparison of the PHSD results with default (without any tunes) PYTHIA 8.2 [22] for $p + p$, $p + n$, $n + n$ collisions from a few GeV to a few TeV. We discuss the production mechanisms of hadrons and role of final state interactions due to the hadronic rescattering. We also show the influence of the possible quark–gluon plasma (QGP) formation on hadronic observables for $p + p$ collisions at the LHC energy.

We stress that the necessity to develop a reliable event generator for the elementary reactions at low and intermediate energies is getting actual and timely since two new HIC accelerators – the Facility for Antiproton and Ion Research (FAIR) in Darmstadt and the Nuclotron-based Ion Collider fAcility (NICA) in Dubna, will become operational in the next years and study nuclear matter at high baryon densities. Moreover, the presently running BES-II (Beam Energy Scan) experiments at RHIC, which includes a fixed target program, provide experimental data in this energy regime.

Our paper is organized as follows: after the Introduction we present the basic ideas of the PHSD approach in Sect. 2, then we step to the "PHSD tune" of the Lund model in Sect. 3 and continue in Sect. 4 with the results for observables and the comparison of the PHSD and PYTHIA results with experimental data for inelastic $p+p$ collisions. We close our paper with summary in Sect. 5.

2 The PHSD approach

We start with brief reminder of the basic ideas of the PHSD transport approach. The Parton–Hadron–String Dynamics transport approach [7–11] is a microscopic off-shell transport approach for the description of strongly interacting hadronic and partonic matter in and out-of equilibrium. It is based on the solution of Kadanoff–Baym equations in first-order gradient expansion [8] employing 'resummed' propagators from the dynamical quasiparticle model (DQPM) [8,23] for the partonic phase.

The DQPM provides an effective description of the properties of the QGP in terms of strongly interacting quarks and gluons with properties and interactions which are adjusted to reproduce lQCD results on the thermodynamics of the equilibrated QGP at finite temperature T and baryon (or quark) chemical potential μ_q. Within the QGP phase, the partons (quarks, antiquarks and gluons) scatter and propagate in a self-generated scalar mean-field potential [9]. On the partonic side the following elastic and inelastic interactions are included $qq \leftrightarrow qq$, $\bar{q}\bar{q} \leftrightarrow \bar{q}\bar{q}$, $gg \leftrightarrow gg$, $gg \leftrightarrow g$, $q\bar{q} \leftrightarrow g$ exploiting 'detailed-balance' with temperature dependent cross sections evaluated at the tree-level with the propagators and couplings from the DQPM.

The expansion of the system leads to a decrease of the local energy density and, once the local energy density becomes close to or lower than $\epsilon_c = 0.5$ GeV/fm^3, the massive colored off-shell quarks and antiquarks hadronize to colorless off-shell mesons and baryons. On the hadronic side, PHSD includes explicitly the baryon octet and decouplet, the 0^--

and 1^--meson nonets as well as selected higher resonances as in the Hadron–String-Dynamics (HSD) approach [12]. In the PHSD approach the full evolution of a relativistic heavy-ion collision, from the initial hard NN collisions out of equilibrium up to the hadronisation and final interactions of the resulting hadronics, is described on the same footing. We recall that this approach has been successfully employed for $p+p$, $p+A$ and $A+A$ reactions from SIS to LHC energies [7–11].

3 Strings in the PHSD

In the PHSD/HSD the string excitation and decay plays a decisive role for inelastic BB, mB, mm collisions in a wide energy range. In the initial phase the high energy hadron–hadron collisions are described by the Lund string model [1,2], where two incoming nucleons emerge the reaction as two excited color singlet states, i.e. 'strings'. A string is characterized by the leading constituent quarks of the incoming hadron as a string ends which are connected by a color flux tubs (color-electric field). The baryonic $(qq-q)$ and mesonic $(q-\bar{q})$ strings are considered with different flavors $(q = u, d, s)$. As the string ends recede, virtual $q\bar{q}$ or $qq\bar{q}\bar{q}$ pairs are produced in the uniform color field by a tunnelling process (described by the Schwinger formula [6]), causing the breaking of the string. The produced quarks and antiquarks recombine with neighbouring partons to "prehadronic" states which will approach hadronic quantum states (mesons or baryon-antibaryon pairs) after a formation time $\tau_F \sim 0.8$ fm/c (in the rest-frame of the string). τ_F is an internal PHSD parameter, introduced in Ref. [24], for controlling the dynamics of "pre-hadronic" states in HIC, it is the same for all energies from SIS to LHC. In the calculational frame of heavy-ion reactions (which is chosen to be the initial NN center-of-mass frame) the formation time then is $t_F = \tau_F \cdot \gamma$, where $\gamma = 1/\sqrt{1-v^2}$ and v is the velocity of the particle in the calculational frame.

The numerical realization of the Lund model in the PHSD is based on the FORTRAN codes FRITIOF 7.02 [3,4], which includes PYTHIA 5.5, JETSET 7.3, ARIADNE 4.02, for energies up to RHIC and PYTHIA 6.4 [5] with the Innsbruck pp tune (390) [25] with CTEQ5 LO PDFs (Jul 2013) for the LHC energies. A smooth transition between both descriptions is realized at "intermediate" energies of $\sqrt{s_{NN}} \leq 250$ GeV. In the PHSD the Lund programs are "tuned", i.e. adjusted in order to get a better agreement with experimental data for elementary collisions.

It is important to stress here that there is *a conceptual difference* in the treatment of 'free' hh reactions (i.e. hh collisions in the vacuum) in the PHSD and PYTHIA (or FRITIOF) beyond the "tuning" of Lund routines: In the PHSD, contrary to PYTHIA, the elementary hh collisions in the vacuum are simulated in a dynamical way, similar to $p+A$ or $A+A$ collisions, i.e. we follow the time evolution of hh reactions – starting from string excitations for high energy hh reactions, to string fragmentations to hadrons, the propagation of hadrons and the dynamical decay of baryonic and mesonic resonances during the expansion of the system. Moreover, the produced hadrons can re-interact elastically and inelastically. The inelastic reactions include the secondary less energetic hh string excitations and low energy hh collisions $2 \rightarrow n$ where $n = 2, 3, 4 \ldots$ [12] as well as multi-meson fusion reactions to baryon-antibaryon pairs and backward reactions ($n\,mesons \leftrightarrow B+\bar{B}$) [26–28]. The Lund routines (FRITIOF and PYTHIA) are used only as event generators for energetic inelastic collisions above a "string threshold" (defined below) which gives us the multiplicity and momentum distribution of produced hadrons. The elastic scattering is realized according to the PHSD routines. Also the decay of resonances – mesonic and baryonic – is realized by the PHSD routines by playing Monte-Carlo for the decay probability with the life-time which is inverse to the total width of the resonance.

Thus, for elementary hh (i.e. BB, mB, mm) reactions in vacuum we solve microscopic transport equations for the propagation in time of all degrees of freedom with a collision term for their interactions. We note here that recently a framework for hadronic rescattering in $p+p$ collisions has been proposed for PYTHIA in Ref. [29]. The inclusion of final state interactions can slightly change the final multiplicity of hadrons as compared to the production point by string decay, as well as their momentum distribution due to elastic scattering as will be discussed in Sect. 4.

We note that all discussed above is relevant for the PHQMD [13] approach, too, since the treatment of the collision integral in the PHQMD is identical to the PHSD. Technically speaking the PHQMD always merges with the latest version of the PHSD and all development in modelling of collisions are incorporated in by the PHQMD automatically. Thus, in this study we will address the PHSD as a main laboratory for testing the string dynamics.

3.1 "PHSD tune" of the string model

Here we discuss the major changes of the Lund codes (FRITIOF 7.02 and PYTHIA 6.4) for their application to the HICs study within the PHSD which we will call as "the PHSD tune":

- We extend the applicability of string routines to lower energies by lowering the threshold from the default value of $\sqrt{s_{min}} = 10$ GeV for the minimal possible energy, to $\sqrt{s_{BB}} = 2.65$ GeV for BB collisions, $\sqrt{s_{mB}} = 2.4$ GeV for mB collisions and $\sqrt{s_{mm}} = 1.3$ GeV for mm collisions. Even going much below the range of the 'default' model applicability, FRITIOF 7.02 and PYTHIA 6.4 give

a very reasonable description of elementary collisions which we will demonstrate in the next section.

- At the string decay, the "flavour chemistry" of the produced quarks is determined via the Schwinger mechanism [6], generalized to $q\bar{q}$ pairs in Refs. [30–32], which defines the production probability of massive $s\bar{s}$ pairs with respect to light flavor $(u\bar{u}, d\bar{d})$ pairs:

$$\frac{P(s\bar{s})}{P(u\bar{u})} = \frac{P(s\bar{s})}{P(d\bar{d})} = \gamma_s = \exp\left(-\pi \frac{m_s^2 - m_{u,d}^2}{2\kappa}\right), \quad (1)$$

with $\kappa \approx 0.176$ GeV^2 denoting the string tension while $m_{u,d,s}$ are the constituent quark masses for strange and light quarks. For the constituent quark masses $m_u \approx 0.35$ GeV and $m_s \approx 0.5$ GeV are adopted in the vacuum which are selected in line with Dyson–Schwinger calculations [33]. From Eq. (1) follows that the production of strange quarks is thus suppressed by a factor of $\gamma_s \approx 0.3$ with respect to the light quarks, which also is the default setting in the Lund routines.
While the strangeness production in proton–proton collisions at SPS energies is reasonably well reproduced with this value, the strangeness yield for $p + Be$ collisions at AGS energies is underestimated by roughly 30% (cf. [34]). For that reason the relative factors used in the PHSD/HSD model are [34]

$$u : d : s : uu = \begin{cases} 1:1:0.3:0.07, & \text{at SPS to RHIC} \\ 1:1:0.4:0.07, & \text{at AGS energies,} \end{cases} \quad (2)$$

with a linear transition of the strangeness suppression factor γ_s as a function of $\sqrt{s_{NN}}$ in between. These settings have been fixed in Ref. [34] for HSD in 1998 and kept since then also for PHSD.

- We modify the flavour decomposition for the production of some mesonic states – $\eta, \eta', \rho, \omega, \phi$ and baryonic states $\bar{p}, \Delta^{++}$ in order to achieve a better agreement with available experimental data in pp collisions. For that we changed the corresponding control parameters in the Lund routines and/or adjusted the hadronic final state directly, e.g. by letting some fraction of produced vector mesons ρ, ω decay to pions (ϕ decay to kaons), i.e. taking the pions (kaons) as a final string decay products – cf. PHSD Refs. [12,35,36].
- The production of all charm and beauty states is realized according to the PHSD routines and not adopted from PYTHIA – cf. [37].
- The production of electromagnetic probes, direct photons and lepton pairs, is treated according to the PHSD routines – cf. [12,36].
- A distribution of the newly produced hadrons in momentum space, i.e. the fraction of energy and momentum that they acquire from the decaying string, is defined by a fragmentation function $f(x, m_T)$. It gives the probability distribution for a hadron with transverse mass m_T to be produced with an energy-momentum fraction x from the fragmenting string:

$$f(x, m_T) \approx \frac{1}{x}(1-x)^a \exp\left(-bm_T^2/x\right), \quad (3)$$

where a, b are parameters. In the PHSD we use $a = 0.23$ and $b = 0.34$ GeV^{-2} [34]. These settings for the string decay to hadrons have been found to match well experimental observations for particle production in $p+p$ and $p+A$ reactions [12].
- In the standard version of FRITIOF/PYTHIA the baryonic and mesonic resonances are produced according to the non-relativistic Breit-Wigner spectral function with a constant width. Moreover, the Breit-Wigner shape is truncated symmetrically around the pole mass, $|M - M_0| < \delta$, with δ chosen 'properly' for each particle such that no problems are encountered in the particle decay chains. In PHSD strings we incorporate the fully relativistic Breit–Wigner spectral functions with mass dependent widths [36]. Also the truncation of the spectral function in mass is removed, i.e. the resonance mass is chosen within the physical thresholds. As before the total energy and momentum conservation holds strictly in the extended Lund routines.

3.2 'In-medium' extension of the Lund string model in the PHSD

PHSD incorporates in-medium effects in the Lund string model, i.e. changes of hadronic properties in a dense and hot environment as created in HICs. The propagation of off-shell hadrons is realized by the Cassing–Juchem off-shell transport equations based on the Kadanoff–Baym equations (cf. the review [8]).

We note that the 'in-medium' modifications are *not used* in our present analysis for pp collisions since the density of baryonic matter is rather low there, however, they become relevant for HIC's where string production happens in a hot and dense environment. Our discussion of 'in-medium' modifications here primarily addresses readers interested in HIC results within the PHSD.

- We incorporate the in-medium spectral functions for mesonic and baryonic resonances in the Lund model by including the density dependent self-energy and in-medium width (depending on the local baryon density and temperature). It allows to study in-medium effects

such as collisional broadening of spectral functions of vector mesons (ρ, ω, ϕ, a_1) [11,36], which is mandatory for the description of dilepton data from HICs. Also it allows to study in-medium effects for the strange mesons $K, \bar{K}$ [38] and strange vector mesons $K^*, \bar{K}^*$ [39–41].

- The chiral symmetry restoration effect (CSR) has been incorporated in the PHSD via the Schwinger mechanism for the string decay in the dense medium which is formed by the primary collisions of nucleons and building of strings during the penetration of the colliding nuclei. In this initial phase a partial restoration of chiral symmetry occurs which leads to a dropping of the scalar quark condensate in the hadronic environment of finite baryon and meson density which can be estimated within the nonlinear $\sigma - \omega$ model. The dropping of the scalar quark condensate leads to a modification of the constituent quark masses for light and strange quarks and thus affect the "chemistry" of decaying strings via the Schwinger mechanism – cf. [42,43]. This leads to an enhancement of strangeness production in the dense baryonic medium before the deconfined phase may occur.
- We take into account the initial state Cronin effect which we model in a dynamical way, i.e. $\langle k_T^2 \rangle$ the average transverse momentum squared of the partons in the nuclear medium created in $p+A$ or $A+A$ collisions, is enhanced due to induced initial semi-hard gluon radiation in the medium, which is not present in the vacuum due to the constraint of color neutrality [44].

4 Comparison of PHSD and PYTHIA 8.2 results for $p+p$, $p+n$, $n+n$ reactions

In this section we present a comparison of the results from the PHSD approach within the "PHSD tune" of strings to the default PYTHIA 8.2 (in 'Soft QCD' mode) [22] for elementary $p+p$, $p+n$ and $n+n$ reactions. We also compare both models to the experimental data when available. We note that in spite that the most experimental data exist for $p+p$ collisions only, it is very important to have reliable results for other isospin channels as $p+n$ and $n+n$ since such reactions are more frequent in HICs due to the larger number of neutrons compared to protons in heavy nuclei. We note that all PHSD results shown here are computed including final state hadronic rescattering (FSI), except of special examples which we will discuss below.

4.1 Hadron multiplicities vs $\sqrt{s_{NN}}$

We start with a comparison of the excitation function of the total multiplicities (i.e. "4π" – without any cuts on rapidity etc.) of $\pi^{\pm}$, $K^{\pm}$, p, $\bar{p}$, K^0_S, $\Lambda + \Sigma^0$ in $p+p$, $p+n$ and $n+n$ collisions as presented in Fig. 1. The PHSD calculations cover the energy range $\sqrt{s_{NN}} = 2.7 - 7000$ GeV and PYTHIA 8.2 – $\sqrt{s_{NN}} = 4 - 7000$ GeV. (We lower the default PYTHIA 8.2 threshold of 10 GeV in view of a closer comparison with the PHSD results). The red lines correspond to $p+p$ collisions, blue lines to $p+n$ reactions and green lines to $n+n$. The PHSD results are drawn with solid lines, PYTHIA 8.2 results with dashed lines. The black dots represent the experimental data for $p+p$ collisions [45–52].

One can see that (i) PYTHIA 8.2 provides systematically larger multiplicities for pions, protons and especially $\bar{p}$. (ii) Furthermore, one can see the rather strong isospin dependence of hadron multiplicities in $p+p$, $p+n$, $n+n$ reactions: the multiplicities of hadrons in $p+p$ reactions are larger than in $p+n$ and $n+n$ reactions. This is demonstrated in Fig. 2 which shows the ratios of $\pi^{\pm}$, $K^{\pm}$, p , $\bar{p}$, K^0_S and $\Lambda + \Sigma^0$ multiplicities in different reactions: the red lines indicate the "$p+n$"/"$p+p$" ratio, while the blue lines the "$n+n$"/"$p+p$" ratio. Here again the solid lines show the PHSD calculations while the dashed lines indicate the PYTHIA results. One can see that both models give very similar ratios which indicate the same flavour decomposition according to isospin channels. The ratios of produced hadrons approach to 1 with increasing energy, i.e. at $\sqrt{s_{NN}} \geq 10 \div 30$ GeV. However, at low energies there is a strong isopin dependence due to the initial combination of charges and flavours.

We continue with Fig. 3 where we show the total ("4π") multiplicity of vector mesons ω, $\rho^{\pm}$, ρ^0, ϕ and strange vector mesons $K^{*\pm}$, K^{*0} produced in $N+N$ collisions: red lines corresponds to $p+p$, blue lines to $p+n$ and green lines to $n+n$ reactions. The PHSD results are drawn by solid lines, the PYTHIA 8.2 results by dashed lines. The black dots represents the experimental data for $p+p$ collisions from Ref. [51]. The isospin dependence is rather weak here in both models. The multiplicities of light vector mesons are lower in PHSD since they were corrected for better matching of existing data. This is also cross-checked by dilepton data for $p+p$ as well as for HICs since the direct decay of vector mesons is one of the dominant channels for dilepton production for invariant masses $0.4 \leq M \leq 1.2$ GeV [11,35]. On the contrary, the multiplicity of strange vector mesons in PHSD is larger at high energies; the description of existing experimental data on K^{0*} total multiplicities at intermediate energies [51] is worth in PHSD than in PYTHIA 8.2. On the other hand, the PHSD p_T spectra of K^* from $p+p$ at midrapidity at RHIC and LHC energies are in a good agreement with experimental data [39–41].

Figure 4 shows the excitation function of the total multiplicity of multi-strange baryons Ω^-, $\bar{\Omega}^+$, Ξ^-, $\bar{\Xi}^+$ produced in $p+p$ collisions. The red lines stand for the PHSD calculations while the blue lines show PYTHIA 8.2 results.

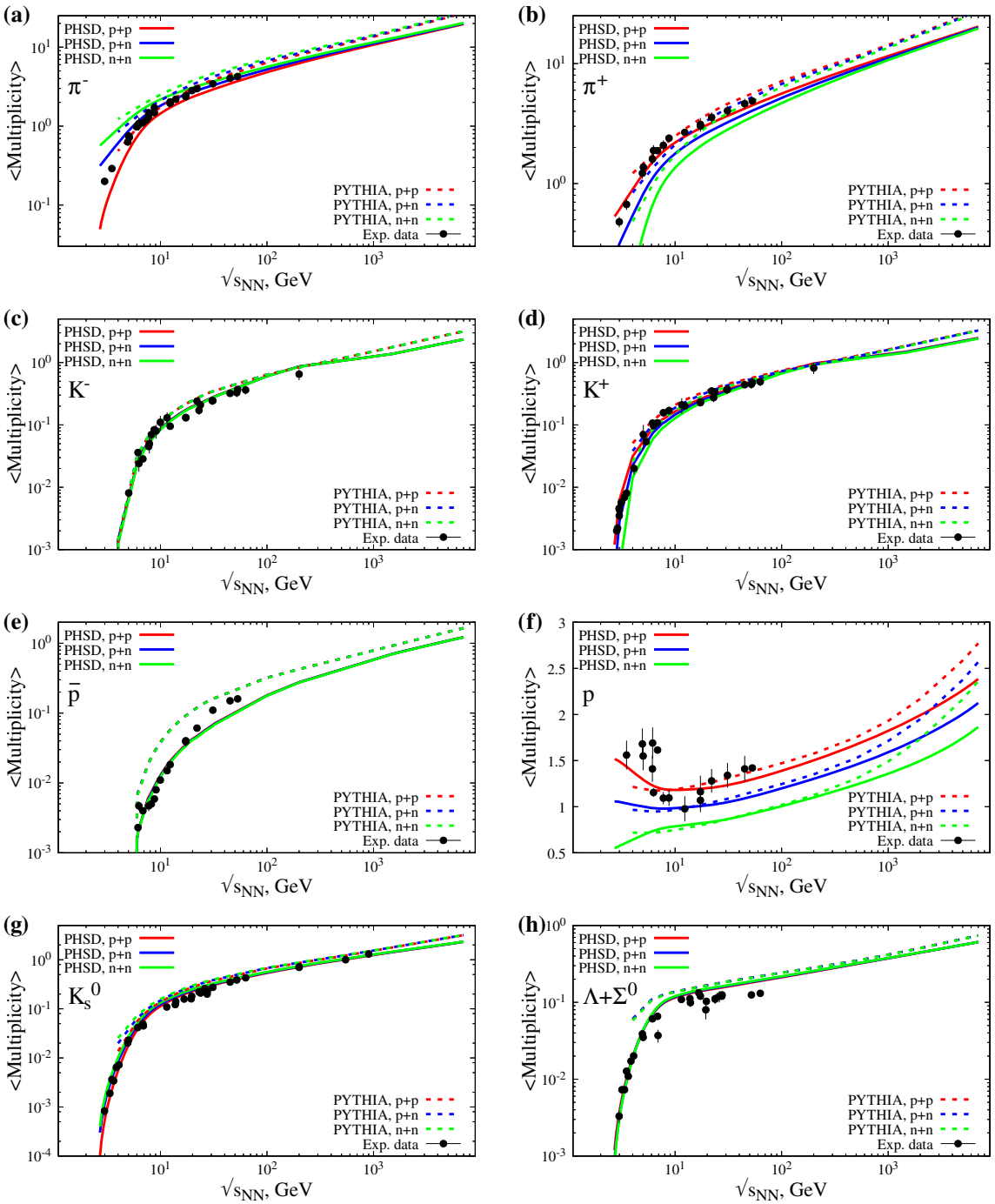

Fig. 1 Total multiplicities of $\pi^{\pm}$, $K^{\pm}$, p , $\bar{p}$, K^0_S and $\Lambda + \Sigma^0$ produced in $N + N$ collisions: red lines corresponds to $p + p$, blue lines to $p + n$ and green lines to $n + n$ reactions. The PHSD results are drawn by solid lines, the PYTHIA 8.2 results by dashed lines. The black dots indicate the experimental data for $p + p$ collisions from Refs. [45–52]

The deviations between both models are rather large at low energies especially for Ω baryons. More "4π" experimental data are needed to construct the multi-strange baryon production.

4.2 Hadronic final state interactions (FSI) in $N + N$ reactions within the PHSD

In order to demonstrate the production mechanisms of the stable final hadrons in PHSD we present in Fig. 5 the channel

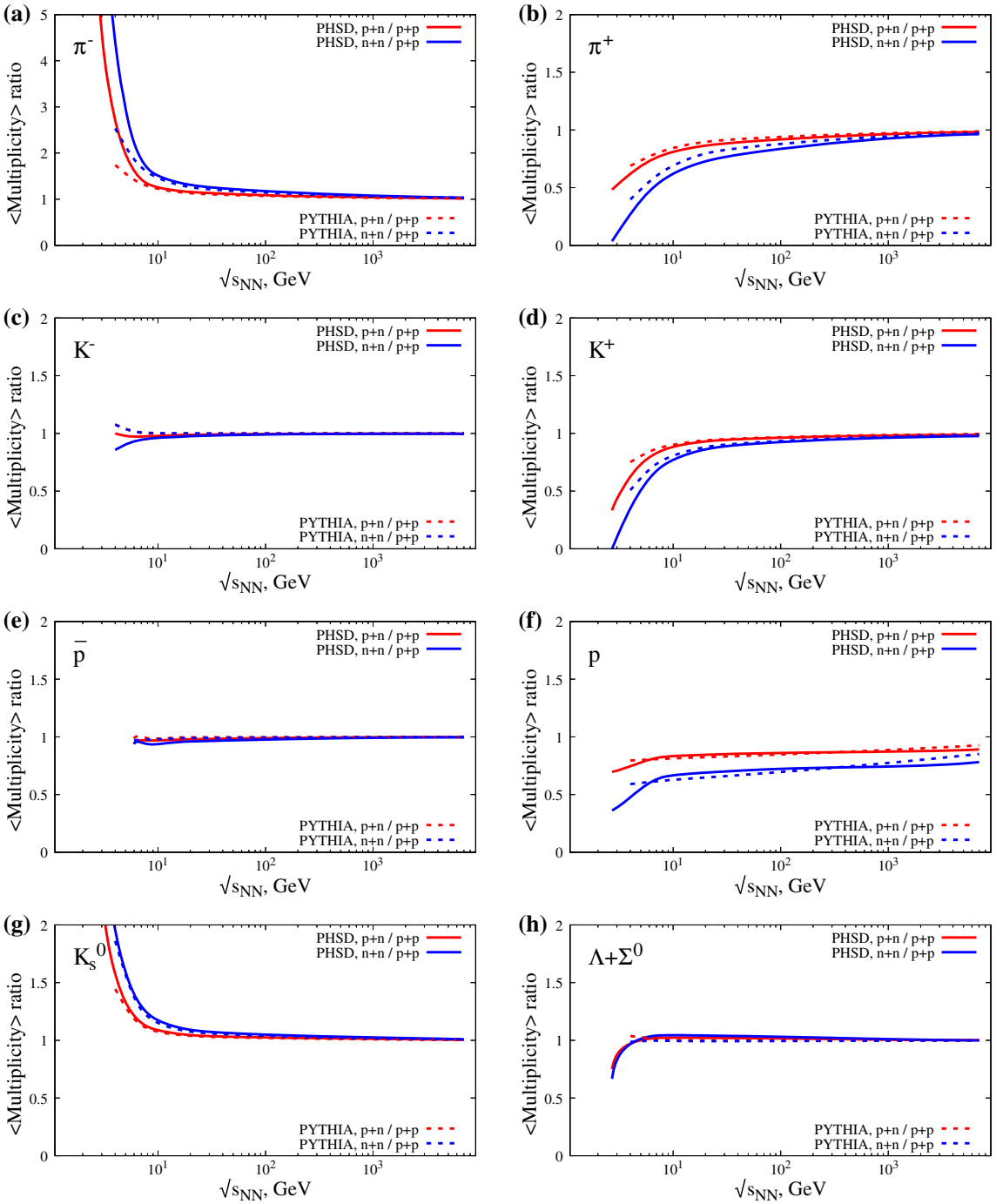

Fig. 2 Ratio of $\pi^{\pm}$ $K^{\pm}$, p , $\bar{p}$, K^0_S and $\Lambda + \Sigma^0$ multiplicities in "$p+n$"/"$p+p$" reactions (red lines) and in "$n+n$"/"$p+p$" (blue lines) calculated within the PHSD (solid lines) and PYTHIA 8.2 (dashed lines)

decomposition for $\pi^{\pm}$ and $K^{\pm}$ production in $p+p$ collisions: The magenta lines ('BB string') show the contribution to the total multiplicity from the direct hadron production from BB string fragmentation, formed by baryon–baryon collisions ($B = p, n, \Delta, \ldots$), the orange lines from secondary mB strings, formed by meson–baryon collisions, while the lines 'Δ, ω, K^*, ρ, ϕ' indicate the contribution from the decay of corresponding resonances. One can see that only about half of the final mesons come directly from BB string fragmentation while the other half comes from resonance decays and even secondary production channels (as mB string, indicated here). Moreover, the produced particles can scatter elastically or participate in charge exchange reactions. Thus, in view of the final state hadronic interactions the dynamics of

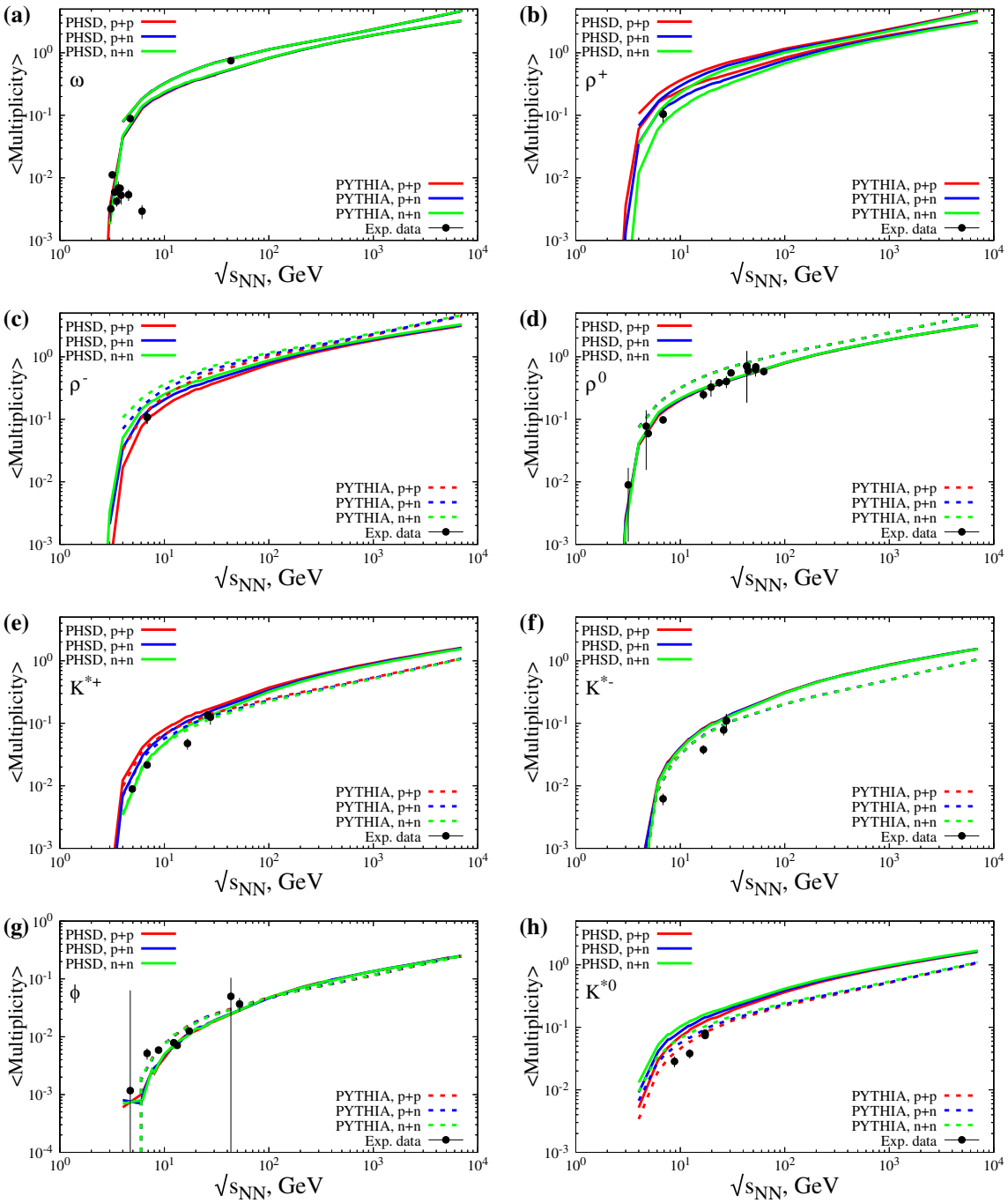

Fig. 3 Total multiplicities of vector mesons ω , $\rho^{\pm}$, ρ^0 $K^{*\pm}$ and ϕ produced in inelastic collisions. The red lines correspond to $p+p$, blue lines to $p+n$ and green lines to $n+n$ collisions. The PHSD results are drawn by solid lines, PYTHIA 8.2 results with dashed lines. The black dots show of the experimental data for $p+p$ collisions [51]

$N+N$ collisions are rather similar to the dynamics of HICs – the hadrons are produced at different times from different sources and not from a single vertex of the initial $N+N$ collision. Indeed, the total multiplicities in $N+N$ is much lower than in HIC at the same energies, i.e. the density of particles is much smaller, correspondingly, the role of final state interactions is strongly reduced.

In order to quantify the role of FSI in elementary $N+N$ reactions we perform PHSD calculations without FSI ('FSIoff') and compute the ratio of total multiplicities with FSI ('FSIon') and without FSI. The results for the ratio

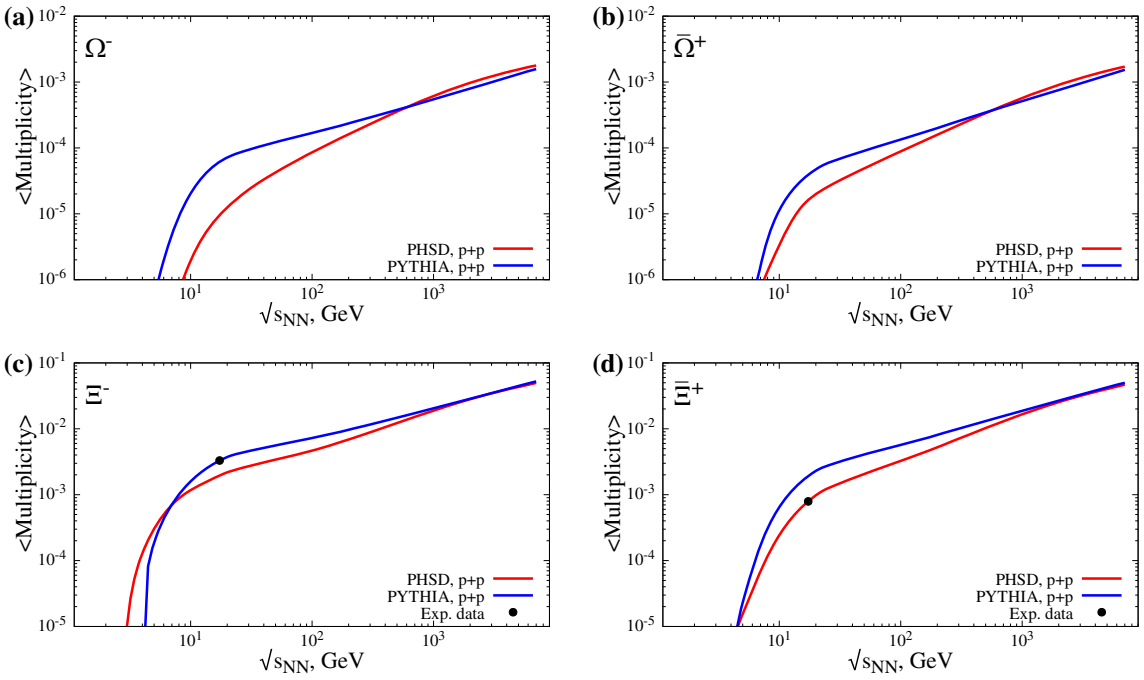

Fig. 4 Total multiplicities of multi-strange baryons Ω^-, $\bar{\Omega}^+$, Ξ^-, $\bar{\Xi}^+$ produced in $p+p$ collisions. The red lines stand for the PHSD calculations while the blue lines shows PYTHIA 8.2 results. The black dots show the NA61/SHINE data [53]

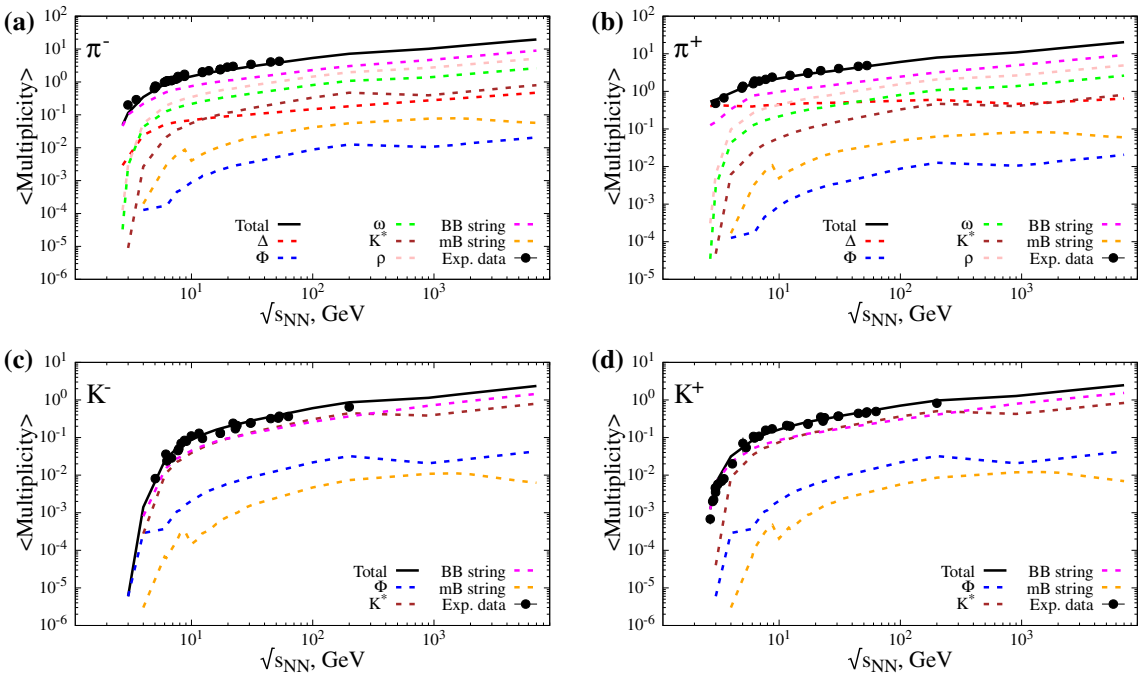

Fig. 5 Channel decomposition for $\pi^{\pm}$ and $K^{\pm}$ production in $p+p$ collisions: The magenta lines ('BB string') show the contribution to the total multiplicity from the direct hadron production from BB string fragmentation, the orange lines from secondary mB strings, while the lines Δ, ω, K^*, ρ, ϕ indicate the contribution from the decay of the corresponding resonances. The black dots indicate the experimental data for $p+p$ collisions from Refs. [45–52]

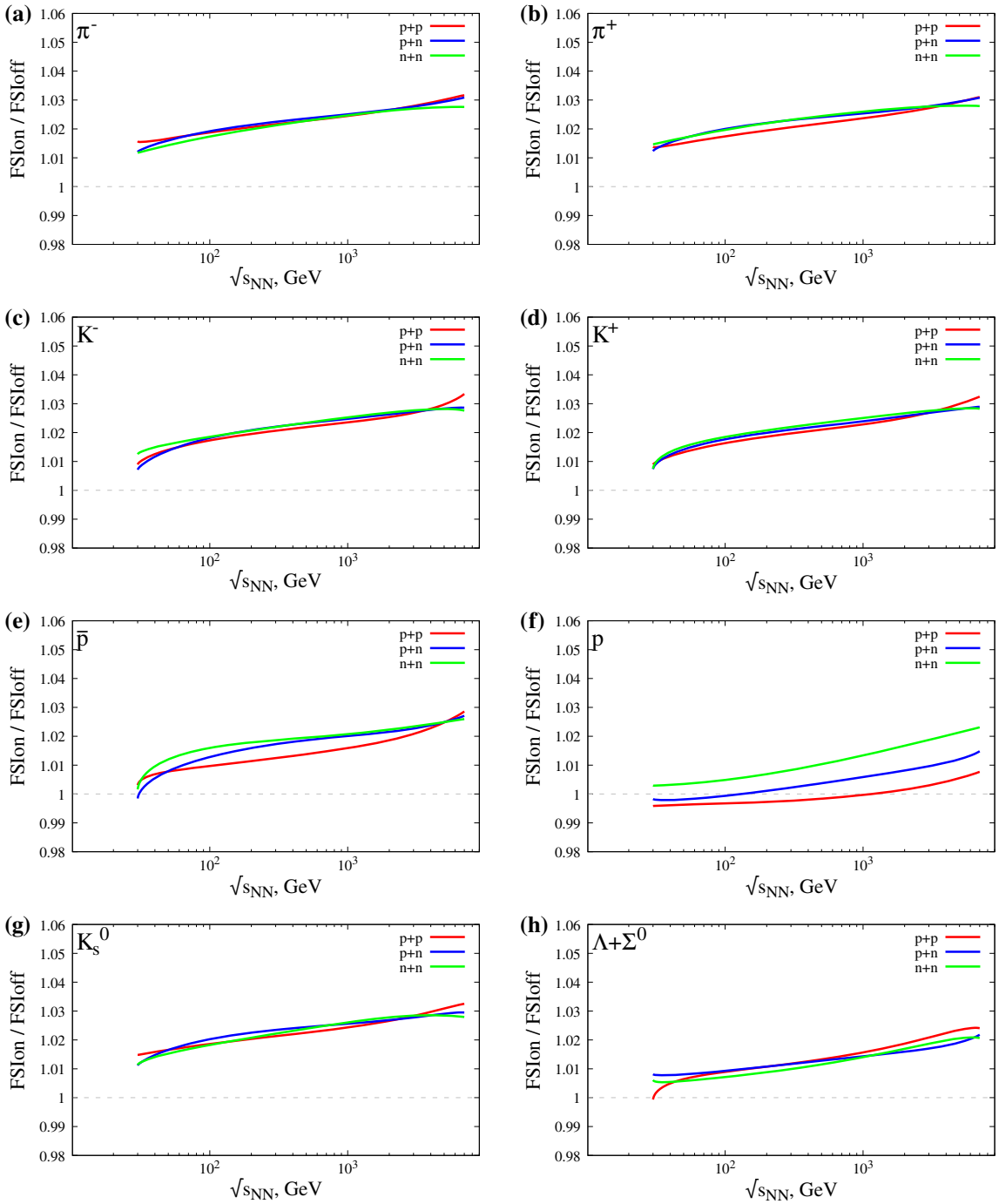

Fig. 6 Ratios of total multiplicities with FSI ('FSIon') and without FSI ('FSIoff') of $\pi^{\pm}$, $K^{\pm}$, p , $\bar{p}$, K_s^0 and $\Lambda + \Sigma^0$ produced in $N + N$ collisions: the red lines correspond to $p + p$, blue lines – to $p + n$ and green lines – to $n + n$ reactions

'FSIon/FSIoff' are presented in Fig. 6 for $\pi^{\pm}$, $K^{\pm}$, p , $\bar{p}$, K_s^0 and $\Lambda + \Sigma^0$ produced in $N + N$ collisions: the red lines correspond to $p + p$, blue lines to $p + n$ and green lines to $n + n$ reactions. One can see that with increasing energy the role of FSI increases and reaches a few percent ($< 5\%$) at the LHC energies. Moreover, the ratios show only a very small dependence on isospin channels $p + p$, $p + n$ or $n + n$.

4.3 x_F distributions at $\sqrt{s_{NN}} = 17.3$ GeV

Now we step on to a comparison of differential observables at different energies.

We start with the comparison of the PYTHIA 8.2 results (orange lines) with the PHSD results (grey lines) and the NA49 data [47,49] on proton x_F distributions (left plot), aver-

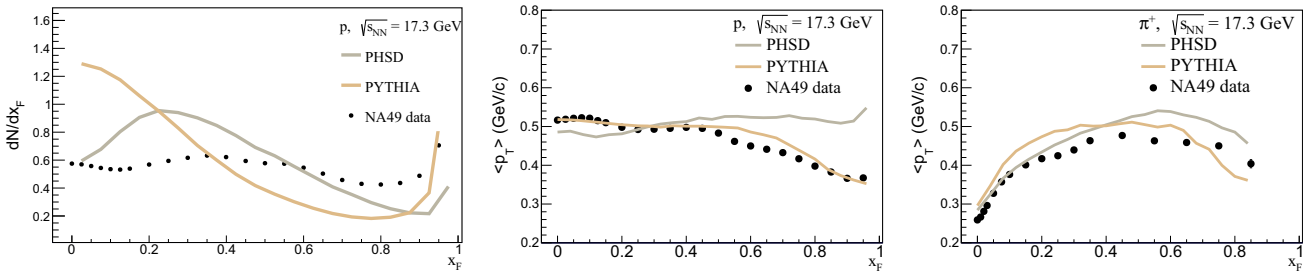

Fig. 7 Proton x_F distribution (left plot) in $p+p$ collisions at $\sqrt{s_{NN}} = 17.3$ GeV. Mean transverse momentum $\langle p_T \rangle$ of protons (middle plot) and π^+ (right plot) as a function of x_F in $p+p$ collisions at $\sqrt{s_{NN}} = 17.3$ GeV. The experimental data are taken from the NA49 Collaboration [47,49]

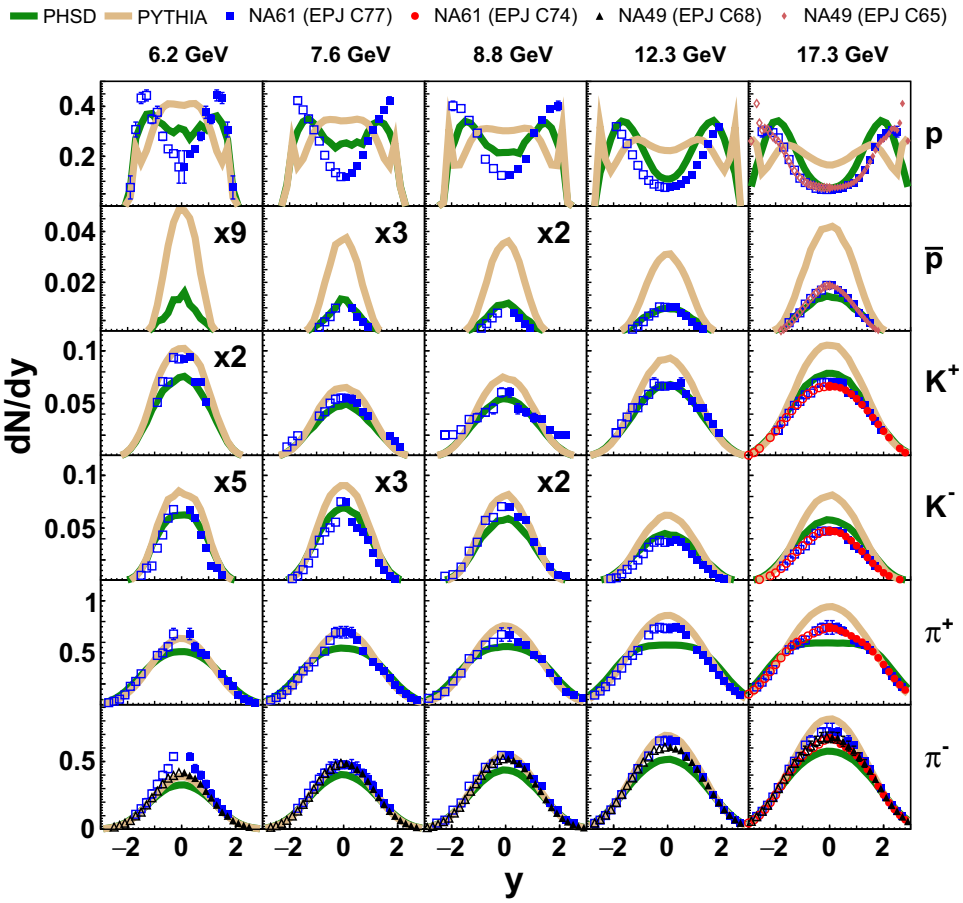

Fig. 8 Rapidity distribution of protons, anti-protons, $K^{\pm}$ and $\pi^{\pm}$ from $p+p$ collisions at 6.2 GeV, 7.6 GeV, 8.8 GeV, 12.3 GeV, 17.3 GeV. The PHSD results are presented by green solid lines while the PYTHIA 8.2 results are shown by brown solid lines. The experimental data are taken from the NA61/SHINE [46] and NA49 [49] Collaborations. The scaling factors for the data and theoretical results are introduced for better visualization: for 6.2 GeV : $\bar{p} \times 9$, $K^+ \times 2$, $K^- \times 5$; for 7.6 GeV : $\bar{p} \times 3$, $K^- \times 3$; and for 8.8 GeV: $\bar{p} \times 2$, $K^- \times 2$

aged transverse momentum $\langle p_T \rangle$ of protons (middle plot) and π^+ (right plot) as a function of x_F in $p+p$ collisions at $\sqrt{s_{NN}} = 17.3$ GeV. One can see that the dN/dx_F spectra are not well reproduced by both models, on the other hand, the $\langle p_T \rangle$ of protons agrees better with PYTHIA while the shape of $\langle p_T \rangle$ of pions is approximately reproduced by both models.

We mentioned that the shape of dN/dx_F distribution of protons is sensitive to the form fragmentation function – Eq. (3). It turns quite non-trivial to fit the parameters in fragmentation function in a way that it describes the experimental data on dN/dx_F distribution at $\sqrt{s_{NN}} = 17.3$ GeV and simultaneously keep the good description on other observables (y, p_T-spectra) at different energies with the same parameters. This require further developments as from theoretical side as well as more experimental information on differential dN/dx_F distribution at different energies.

4.4 Comparison of rapidity distributions at $\sqrt{s_{NN}} = 6.2-17.3$ GeV

We continue with a comparison of the PHSD and PYTHIA 8.2 results to the experimental data from the NA49 and NA61/SHINE Collaborations on rapidity distributions dN/dy of protons, antiprotons, $\pi^{\pm}$, $K^{\pm}$ at $\sqrt{s_{NN}} = 6.2$, 7.6, 8.8, 12.3, 17.3 GeV which are shown in Fig. 8. The data from the

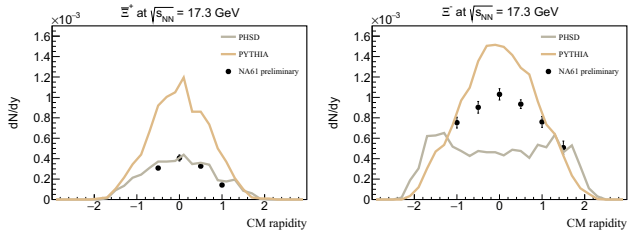

Fig. 9 Rapidity distribution of $\bar{\Xi}^+$ (left plot) and Ξ^- (right plot) from $p+p$ collisions at 17.3 GeV. The PHSD results are presented by gray solid lines while the PYTHIA 8.2 results are shown by brown solid lines. The experimental data are taken from the NA61/SHINE Collaboration [53]

NA61/SHINE [45,46] and NA49 [47–49] Collaborations are drawn by solid symbols, the open symbols indicate the data reflected about midrapidity. The PHSD results are plotted by solid lines. There are no experimental data for antiprotons below 8.8 GeV. Additionally, Fig. 9 shows the comparison of model calculations for the rapidity distribution dN/dy as a function of center-of-mass rapidity y of $\bar{\Xi}^+$ (left plot) and Ξ^- (right plot) from $p+p$ collisions at 17.3 GeV to the experimental data from the NA61/SHINE Collaboration [53].

The model discrepancies with respect to the experimental data on the dN/dy distributions of newly produced hadrons can be attributed to a large extend to the description of proton "stopping", i.e. to the shape of the rapidity distribution of protons. PYTHIA 8.2 tends to have much stronger stopping at all considered energies, the proton dN/dy distributions are rather flat at midrapidity while the PHSD results show minima at midrapidity and a rise at target/projectile rapidity in line with the experimental data. Thus, the hadronic rapidity distributions from PYTHIA 8.2 systematically overestimate the data while the PHSD results are closer to the data. However, this correlation is not so direct, e.g. the PYTHIA results are perfectly on the data for π^- at $\sqrt{s_{NN}} = 6.2, 7.6, 8.8, 12.3$ GeV while PHSD underestimates the data. The same holds for the description of multi-strange baryons $\bar{\Xi}^+$and Ξ^- in Fig. 9. The latter require further improvements on the mechanisms of multi-strangeness production at such intermediate energies.

4.5 Comparison of transverse momentum p_T spectra at $\sqrt{s_{NN}} = 6.2 - 17.3$ GeV

Figure 10 shows the transverse momentum distributions of protons, π^-, $K^\pm$ from inelastic $p+p$ collisions at $\sqrt{s_{NN}} =$

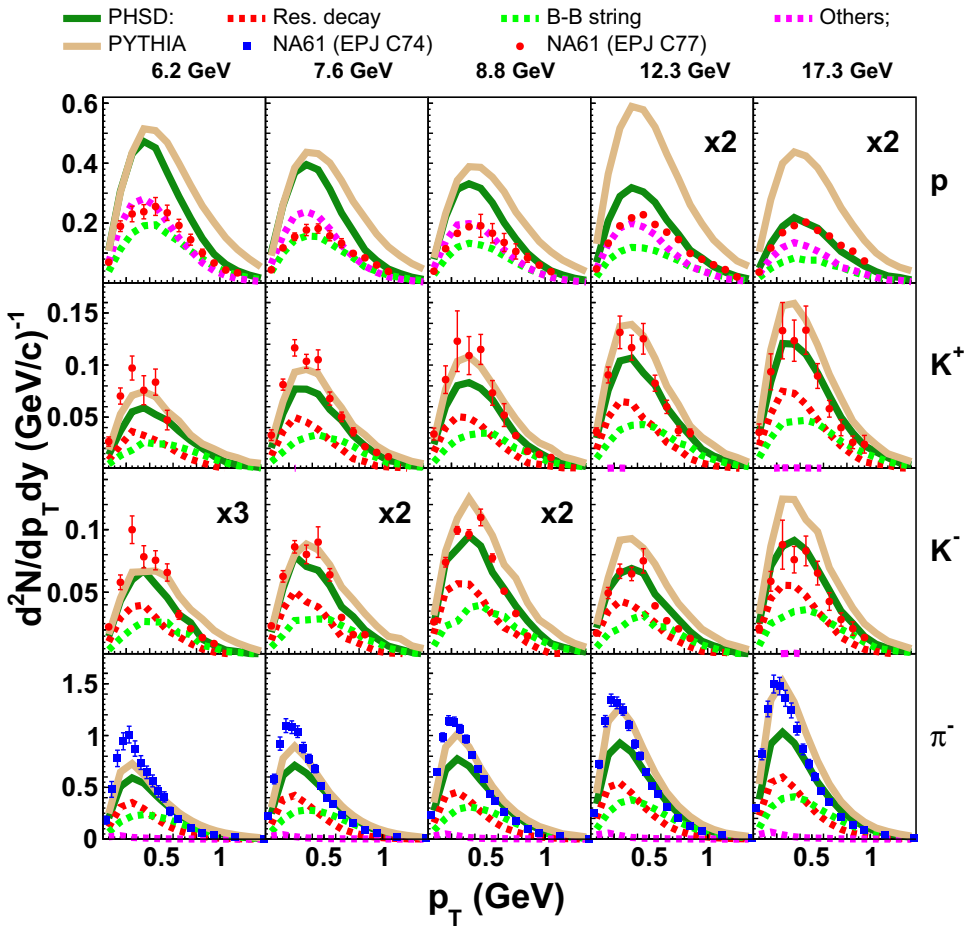

Fig. 10 Transverse momentum spectra of protons, K^+, K^- and π^- from $p+p$ collisions in the central midrapidity interval $0 < y < 0.2$ at 6.2 GeV, 7.6 GeV, 8.8 GeV, 12.3 GeV, 17.3 GeV. The PYTHIA 8.2 results are plotted by brown solid lines, the PHSD results are presented by green solid lines. The channel decomposition of the PHSD results are also shown: the contribution from the hadrons coming directly from the decays of BB strings is plotted by light green dash-dotted lines while those coming from baryonic or mesonic resonance decays are drawn by red dash lines, the magenta lines show the sum distribution form "other" sources during the final state interaction. The experimental data are taken from the NA61/SHINE Collaboration [46]. The scaling factors for the data and theoretical results are introduced for better visualization: $K^-\times 3$ for 6.2, 7.6, 8.8 GeV; $\bar{p}\times 3$ for 12.3, 17.3 GeV

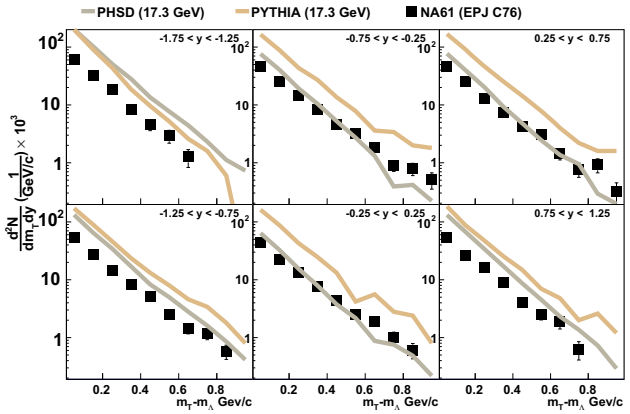

Fig. 11 Transverse mass m_T spectra of $\Lambda + \Sigma^0$ for different rapidity intervals ($-1.75 \le y \le -1.25$, $-0.75 \le y \le -0.25$, $0.25 \le y \le 0.75$, $-1.25 \le y \le -0.75$, $-0.25 \le y \le 0.25$, $0.75 \le y \le 1.25$) from $p + p$ collisions at 17.3 GeV. The PYTHIA 8.2 results are plotted by brown solid lines, the PHSD results are presented by gray solid lines. The experimental data are taken from the NA61/SHINE Collaboration [54]

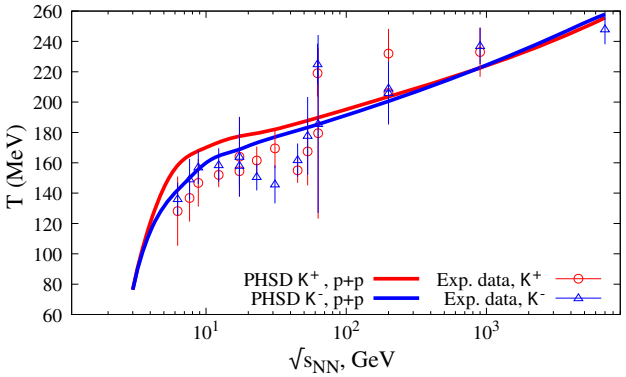

Fig. 12 The inverse slope parameter T of the m_T-spectra of $K^{\pm}$ mesons at mid-rapidity within the PHSD model. The compilation of experimental data are taken from [55]

6.2, 7.6, 8.8, 12.3, 17.3 GeV. The experimental data from the NA61/SHINE Collaboration [45,46] are drawn by symbols, the spectra are measured near midrapidity ($0 < y < 0.2$). The PHSD results are plotted by green solid lines, while the PYTHIA 8.2 by brown solid lines. We also show the contributions from different channels for the PHSD spectra: the contribution from the hadrons coming directly from the decays of BB strings is plotted by light green dash-dotted lines while those coming from the baryonic or mesonic resonance decays are drawn by red dash lines, the magenta lines show the contribution form "other" sources during the final state interaction. As one can see the latter is rather small for all hadron species. The hadrons stemming from string decay show much harder spectra than from resonance decays which fill the low part of the p_T distributions.

In Fig. 11 we show the comparison of the PHSD and PYTHIA results for the transverse mass m_T spectra for the strange baryons $\Lambda + \Sigma^0$ for different rapidity intervals at $\sqrt{s_{NN}}$ =17.3 GeV in comparison to the data from the NA61/SHINE Collaboration [54]. In spite that the absolute values of the m_T spectra are overestimated by PYTHIA 8.2 for all rapidity bins (for the reasons discussed in Sect. 4.4), the slope of the theoretical spectra is approximately in line with the experimental data; the PYTHIA slopes are slightly harder than the PHSD slopes.

4.6 Excitation function of the inverse slope parameter of the m_T- spectra of $K^{\pm}$ mesons

Strangeness production in $A + A$ and $p + p$ collisions are always in the focus of the theoretical and experimental interest: the measured inverse slope T of the m_T spectra of $K^{\pm}$ mesons defined as

$$\frac{1}{m_T}\frac{dN}{dm_T} \sim \exp\left(-\frac{m_T}{T}\right) \tag{4}$$

shows a "step" behaviour in central $A + A$ collisions from 20 to 160 A·GeV energies. This substantial flattening of the spectra in central Au + Au collisions relative to $p + p$ interactions has been attributed to the onset of a deconfinement transition from hadronic to partonic matter [56,57]. As has been shown in Ref. [58] such collective behaviour could not be reproduced by hadron based models (as HSD or UrQMD) and might indicate the creation of pressure by partonic interactions in HICs [7].

In the last decade the experimental knowledge on the m_T spectra of $K^{\pm}$ in $p + p$ collisions has been improved. Thus, we update and extend our previous study of the inverse slope parameter T of the midrapidity m_T spectra of $K^{\pm}$ mesons (cf. [58]) and present in Fig. 12 the PHSD result for the excitation function of T versus $\sqrt{s_{NN}}$. The compilation of the worldwide experimental data are taken from [55]. One can see that PHSD reproduces the $K^{\pm}$ slope rather well in a very wide energy range from a few GeV to a few TeV.

4.7 Comparison of y- and p_T-distributions at $\sqrt{s_{NN}} = 200$ GeV

Now we step to ultra-relativistic energies and compare the PHSD and PYTHIA 8.2 results with data from the STAR [59] and PHENIX [60] Collaborations in Fig. 13. One can see that the experimental data on meson spectra are rather well reproduced by both models while the spectra of $\Lambda + \Sigma^0$ are slightly underestimated and $\bar{\Lambda} + \bar{\Sigma}^0$ spectra are overestimated. The agreement between PHSD and PYTHIA is quite good except of the low p_T region for the baryons where the PYTHIA spectra are higher than the PHSD ones.

The latter is also observed in the differential cross section $d\sigma/d\eta$ of negatively-charged hadrons versus pseudorapidity

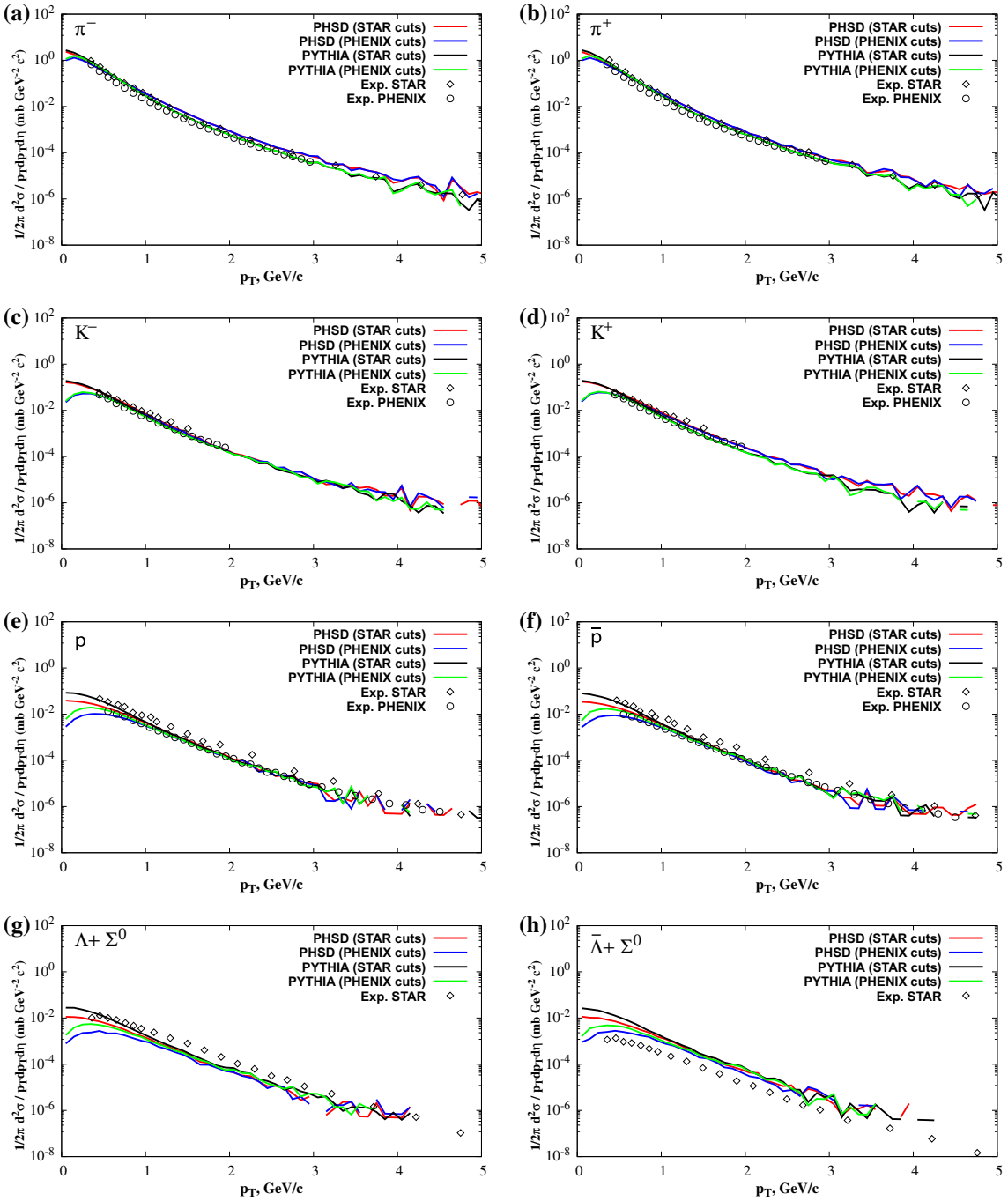

Fig. 13 The invariant yields of π^+, K^+ p, $\Lambda + \Sigma^0$ and $\bar{\Lambda} + \bar{\Sigma}^0$ as a function of p_T. The cuts $|y| < 0.5$ and $|\eta| < 0.35$ were applied to the models for a comparison with STAR [59] (open rhombus) and PHENIX [60] (open circles) data accordingly. The PHSD results with STAR y-cut are shown as the red solid lines, with the PHENIX η-cut as blue solid lines. The PYTHIA 8.2 results with STAR y-cut are shown by the black dashed lines, with the PHENIX η-cut by green dashed lines

η presented in the left part of Fig. 14. Here the PYTHIA result overestimates the experimental data from the UA5 Collaboration [61] at mid-η while PHSD agrees very well with data. In Fig. 14 the PHSD results are shown for two cases: including the FSI (default for this study) by the red lines ('PHSD-FSIon') and without FSI by the blue lines ('PHSD-FSIoff'). The right part of Fig. 14 presents the invariant cross-section of charged particles for $|\eta| < 2.5$ versus p_T. One sees that the p_T spectra from the PHSD are harder at large p_T and slightly softer at very low p_T. The latter can not be attributed

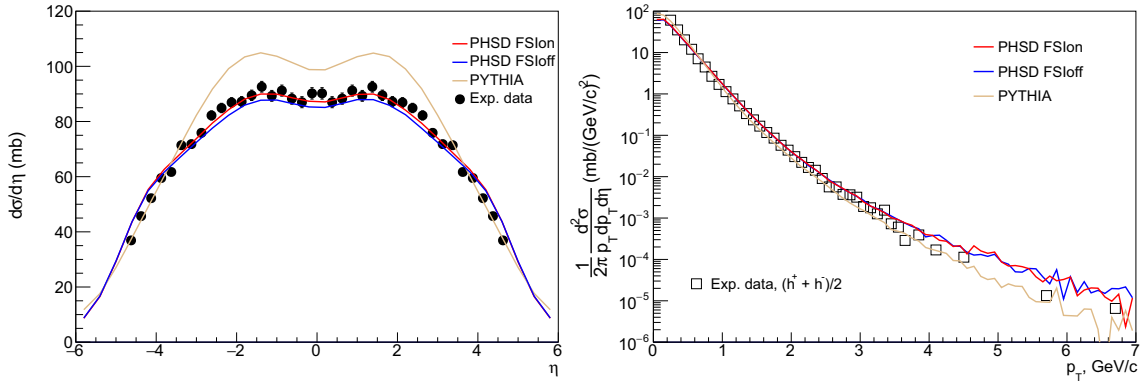

Fig. 14 Left: the differential cross section $d\sigma/d\eta$ of negatively-charged hadrons versus pseudorapidity η. Right: the invariant cross-section of charged hadrons for $|\eta| < 2.5$ versus p_T. The PYTHIA 8.2 results are displayed by the brown lines. The PHSD results are shown for two cases: including the FSI (default) by the red lines ('PHSD-FSIon') and without FSI by the blue lines ('PHSD-FSIoff'). The experimental data from the UA5 and UA1 Collaborations are taken from Refs. [61,62]

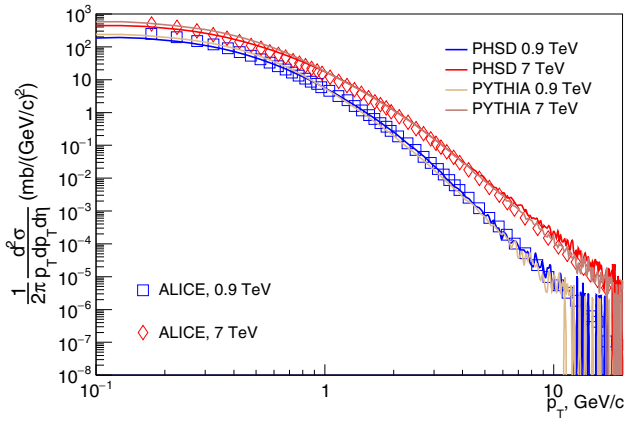

Fig. 15 The invariant cross section versus p_T for charged particles for $|\eta| < 0.8$ for $p + p$ collisions at invariant energies $\sqrt{s_{NN}}$ =0.9 TeV and 7 TeV. The PHSD results are indicated by the blue line for 0.9 TeV and by the red line for 7 TeV. The PYTHIA 8.2 results are shown by the brown line for 0.9 TeV and by the grey line for 7 TeV. The experimental data from the ALICE Collaboration [63] at 0.9 TeV are shown as open rhombus and at 7 TeV as open squares

to the FSI during the expansion rather than to the differences in string fragmentation since the PHSD results with and without FSI are very close to each other in the whole p_T range. The FSI leads to a very small enhancement of the hadron multiplicity at mid-rapidity which has been also shown in Fig. 6.

4.8 Comparison of p_T spectra at LHC energies, traces of the final state interactions

We increase in energy up to the LHC now and come to a comparison of the PHSD and PYTHIA 8.2 results to the ALICE data. In Fig. 15 the invariant cross section versus p_T for charged particles for $|\eta| < 0.8$ for $p + p$ collisions at invariant energies $\sqrt{s_{NN}}$ =0.9 TeV and 7 TeV are shown. The PHSD results are indicated by the blue line for 0.9 TeV and by the red line for 7 TeV. The PYTHIA 8.2 results are shown by the brown line for 0.9 TeV and by grey line for 7 TeV. The experimental data from the ALICE Collaboration [63] at 0.9 TeV are shown as open rhombus and at 7 TeV as open squares. One can see that the PHSD and PYTHIA p_T distributions have a similar slope, however, the PYTHIA spectra are slightly higher. Both models are in a good agreement with ALICE data which cover 10 orders of magnitude in range.

We continue with a model comparison of transverse momentum spectra of identified hadrons in $p + p$ collisions to the spectra measured by the ALICE Collaboration [64] at 7 TeV. At such ultra-relativistic energy a large amount of hadrons are produced during the string breaking which leads to large energy-density fluctuations and to the possible creation of small droplets of QGP especially in the events with very high multiplicities. The experimental observation of a visible v_2 (which is even comparable with the v_2 of heavy-ions) in high multiplicity $p + p$ collisions [66] indicates the development of collective effects (i.e. hydrodynamic behaviour) in such small system [19,67,68] which might be also in line with the idea of QGP formation in high multiplicity $p + p$.

In order to study the possible traces of the QGP formation on hadronic 'bulk' observables – as p_T spectra – we perform PHSD calculations when additionally to the hadronic final state interactions (default), we consider the formation of the QGP after the initial pp string breaking in a similar way as in HICs (cf. Sect. 2). Indeed, the QGP formation in $p+p$ might happen only in a few cells where, due to fluctuations, the local energy density becomes larger than the critical $\varepsilon_C \simeq 0.5$ GeV/fm^3 such that a dissociation of hadrons to partons occurs in this cell. However, the size and the life time of such QGP

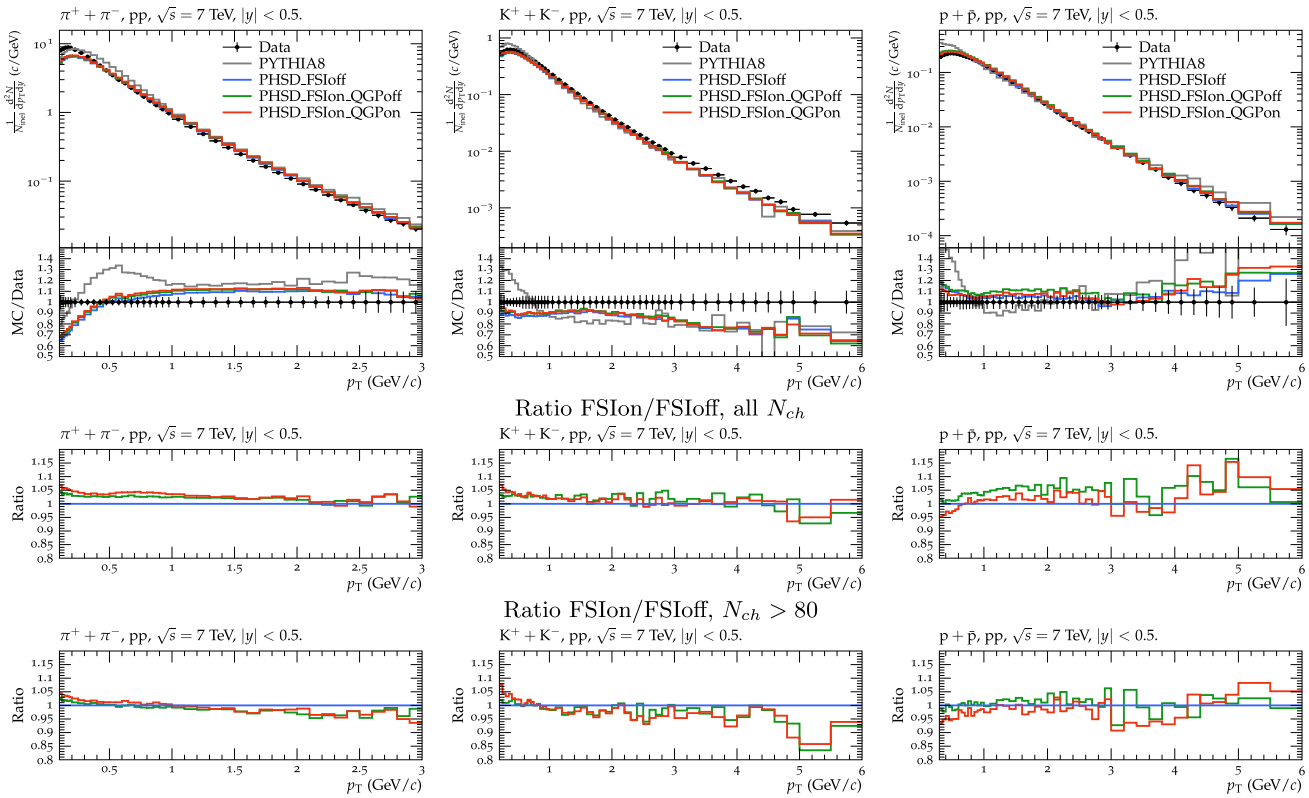

Fig. 16 Upper row: the transverse momentum spectra of $\pi^+ + \pi^-$ (left), $K^+ + K^-$ (middle), and $p + \bar{p}$ (right) in midrapidity ($|y| < 0.5$) $p + p$ collisions at $\sqrt{s_{NN}} = 7$ TeV. The grey lines correspond to the PYTHIA 8.2 results, the blue lines to the PHSD results without FSI ('PHSD-FSIoff'), the green lines to the PHSD results with hadronic FSI, but without QGP creation ('PHSD-FSIon-QGPoff'), the red lines to the PHSD results with hadronic FSI and with QGP creation ('PHSD-FSIon-QGPon'). The solid dots indicate the experimental data from the ALICE Collaboration [64]. The deviation of the model results from the data are shown directly under each plot. Middle row: the ratio of the PHSD transverse momentum spectra (from the upper plots) calculated with hadronic FSI but without QGP creation to the spectra without FSI (FSIon-QGPoff/FSIoff) shown by green lines, with FSI with QGP to the spectra without FSI (FSIon-QGPon/FSIoff) by red lines. Lower row: the same as middle, but for number of charge particles $N_{ch} > 80$. The analysis is performed using Rivet [65]

droplets are very small contrary to HICs, they carry only a very small fraction of the total energy in the collisions, thus, one could not expect a larger effect of the QGP creation on bulk observables.

In Fig. 16 we show the p_T spectra of $\pi^+ + \pi^-$ (left panel), $K^+ + K^-$ (middle panel), and $p + \bar{p}$ (right panel) in midrapidity ($|y| < 0.5$) $p + p$ collisions at $\sqrt{s_{NN}} = 7$ TeV. The grey lines correspond to the PYTHIA 8.2 results, the blue lines to the PHSD results without FSI ('PHSD-FSIoff'), the green lines to the PHSD results with hadronic FSI, but without QGP creation ('PHSD-FSIon-QGPoff'), the red lines to the PHSD results with hadronic FSI and with QGP creation ('PHSD-FSIon-QGPon'). The analysis is performed using Rivet [65] which allows to show the deviation of the models from the experimental data below each plot. One can see that PYTHIA 8.2 creates more very low momentum hadrons than the PHSD (which we attribute to the Innsbruck tune of string routines used in the PHSD). With increasing p_T both models show a similar trend: pion $\pi^+ + \pi^-$ spectra are slightly harder in the models while $K^+ + K^-$ spectra are softer; the $p + \bar{p}$ spectra agree very well with data up to 5 GeV/c.

In order to quantify the role of the final state interactions we show additionally the ratios of the PHSD transverse momentum spectra (from the upper plots) calculated with hadronic FSI but without QGP creation to the corresponding spectra without FSI (FSIon-QGPoff/FSIoff) by the green lines in the middle row; with FSI with QGP to the spectra without FSI (FSIon-QGPon/FSIoff) by red lines. The lower row indicates the same ratios as the middle row, but for the number of charged particles $N_{ch} > 80$, i.e. by selecting the events with large multiplicities. One can see from Fig. 16 that the FSI effect is relatively small, on the level of 5% in average. This PHSD result is consistent with a recent finding by Sjöstrand and Utheim [29] who incorporated the framework for accounting of the FSI in PYTHIA in terms of hadronic rescattering.

As follows from Fig. 16, the PHSD calculations with the hadronic FSI as well as with hadronic FSI and QGP creation

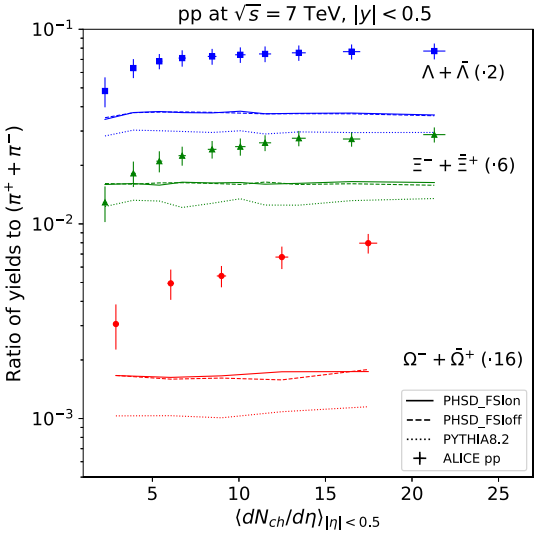

Fig. 17 The ratio of the p_T-integrated yield of $\Lambda + \bar{\Lambda}$ (multiplied by a factor 2), $\Xi^- + \bar{\Xi}^+$ (multiplied by 6), $\Omega^- + \bar{\Omega}^+$ (multiplied by 16) to pions $(\pi^+ + \pi^-)$ as a function of $dN_{ch}/d\eta$ for $|y| < 0.5$ at $\sqrt{s_{NN}} = 7$ TeV. The dotted lines correspond to the PYTHIA 8.2 results, the dashed lines to the PHSD results without FSI ('PHSD-FSIoff'), the solid lines to the PHSD results with hadronic FSI ('PHSD-FSIon'). The experimental data from ALICE Collaboration are taken from Ref. [69]

lead to a small softening of the low p_T pion and kaon spectra and hardening of proton+antiproton spectra. This is attributed to elastic scattering (which has a forward peaked angular distribution for $B + B$ and $m + B$ collisions) as well as to the inelastic processes and formation of resonances (dominantly Δ's). The high p_T region is less sensitive to the FSI.

4.9 Comparison of multi-strangeness production at LHC energies

Finally, we step to the multi-strangeness production in pp reactions and compare in Fig. 17 the PHSD and PYTHIA 8.2 results for the ratio of the p_T-integrated yield of $\Lambda + \bar{\Lambda}$ (multiplied by a factor 2), $\Xi^- + \bar{\Xi}^+$ (multiplied by 6), $\Omega^- + \bar{\Omega}^+$ (multiplied by 16) to pions $(\pi^+ + \pi^-)$ as a function of $dN_{ch}/d\eta$ for $|y| < 0.5$ at $\sqrt{s_{NN}} = 7$ TeV with the ALICE data from Ref. [69] (we keep the multiplication factors as in Fig. 2 of Ref. [69] for easy comparison). We mention that the analysis has been performed using Rivet. As seen from Fig. 17, both models can not reproduce the enhancement of multi-strange baryon production compared to the non-strange hadrons in high multiplicity events as observed by the ALICE Collaboration. As follows from the PHSD results with and without the hadronic FSI, the final rescattering on the hadronic level can not enhance the ratio since the "chemistry production" is mainly attributed to the very initial stages of pp collisions. The "QGP" scenario (we omit to show it explicitly in Fig.17 since it is similar to the other scenarios within statistical fluctuations) in PHSD also can not make it since (as explained above) the QGP is formed by melting the "pre-hadrons" during the expansion phase and the QGP droplets can be formed due to the fluctuations in energy density. Thus, the PHSD and PYTHIA 8.2 results are qualitatively close to each other, the differences between them can be attributed to the different settings for the strange diquark production.

We note that the enhancement of strange to non-strange hadron production in pp reactions has been reproduced within the EPOS-LHC model [19] by the collective hadronization of hot 'core' which decays in a statistical way to hadrons as well as by the DIPSY Monte-Carlo event generator in Ref. [70] by introducing 'colour ropes'. Such mechanisms are not incorporated in the default PYTHIA 8.2 and in the PHSD.

5 Summary

We have studied the hadron production in $p + p$, $p + n$ and $n + n$ reactions within the PHSD which is a microscopic transport approach for the dynamical description of $A + A$ and $p + A$ collisions and compared the PHSD results with PYTHIA 8.2. In the PHSD the time evolution of collisions is described by the solution of generalized transport equations derived from the first-order gradient expansion of Kadanoff–Baym equations applicable for strongly interacting systems. In the PHSD all interactions in the system – on a hadronic or partonic levels – are treated in a fully microscopic way. The multiparticle production from the primary energetic NN collisions as well as from secondary BB, mB and mm reactions are based on the Lund string model realized in terms of the event generators FRITIOF and PYTHIA.

The Lund event generators FRITIOF and PYTHIA have been developed with the focus on elementary reactions at ultra-relativistic energies. However, the FRITIOF and PYTHIA generators are very important also for the description of heavy-ion physics since they historically have been incorporated in many transport approaches. Such applications to HICs requires from elementary event generators a good description of BB, mB and mm reactions in very wide energy range – from few GeV to a few TeV. Moreover, the flavour "chemistry" of elementary reactions, happening during the time evolution of HICs, covers all possible flavour combinations of the colliding hadrons. Additionally, the hh interactions in HICs are happening in a hot and dense environment and not in vacuum as in "free" $p + p$ collisions. This requires a modification ("tune") of the original Lund string model which we have presented here within the PHSD approach.

The **"PHSD tune"** of the Lund string model (FRITIOF 7.02 and PYTHIA 6.4 generators) contains of few basic directions which could be summarized as

(I) an improvement of the description for the elementary reactions in the vacuum:

- an extension of the applicability range of the Lund generators to very low energies
- an improvement on the flavour "chemistry" of produced hadrons
- a modification of the string fragmentation function, i.e. in energy-momentum distributions for a better description of low energy data on hadron production

(II) a modification of string fragmentation and the properties of produced hadrons in the hot and dense medium created in HICs:

- an implementation of chiral symmetry restoration via the Schwinger mechanism for string decay in the dense medium
- accounting for the initial state Cronin effect for $\langle k_T \rangle$ broadening in the medium
- implementation of the in-medium properties of hadrons in the string fragmentation by incorporation of the in-medium spectral functions for mesonic and baryonic resonances with momentum, density and temperature dependent widths instead of non-relativistic spectral functions with constant width.

(III) We also pointed out the conceptual difference in the treatment of free (i.e. in the vacuum) $N + N$ collisions between the PHSD and PYTHIA models. In the default PYTHIA 8.2 the hadrons are produced by the string fragmentation which provides the momenta of outgoing particles, however, the space-time picture of $p + p$ collisions is not presented here. In the PHSD the free $N + N$ collisions are treated in a similar fashion as in $A + A$, i.e. following the space-time and momentum evolution of the system by solving the relativistic transport equations of motion. Moreover, the hadrons produced from primary string fragmentation can participate in the final state interactions by hadronic rescattering. Furthermore, at ultra-relativistic collisions small droplets of QGP could be formed in events with a high multiplicity of produced hadrons due to energy-density fluctuations.

In this study we have presented a detailed comparison of the PHSD results with those from the default version of PYTHIA 8.2 for 'bulk' observables such as the excitation functions of hadron multiplicities as well as differential rapidity y, transverse momentum p_T and x_F distributions in $p + p$, $p + n$ and $n + n$ reactions in the energy range $\sqrt{s_{NN}} = 2.7 - 7000$ GeV where we also compared the models with the existing experimental data.

We found that (i) in general the extrapolation of the Lund model (realized by the FRITIOF, PYTHIA generators) to low energies (much below the default threshold) works rather well for the description of total multiplicities of produced hadrons which validates its use as elementary event generators in transport approaches. However, some tuning is still required; the experimental data on the multiplicities of produced hadrons at low and intermediate energies are better described with the "tuned strings" in PHSD. The same holds for the differential observables as rapidity and p_T spectra. However, a further improvement of the string fragmentation is required in order to obtain a better description of experimental data at low and intermediate energies, especially for the production of multi-(anti-)strange hadrons.

(ii) We showed a strong isospin dependence of particle production in $p + p$, $p + n$ and $n + n$ reactions, especially at low energies. However, the lack of experimental data doesn't allow to make reliable constrains here. In this respect experimental data on proton + light nuclei collisions might be helpful.

(iii) We have investigated the role of final state interactions due to the hadronic rescattering on the bulk observables and found that at low energies it is negligible due to a very low density of produced hadrons; the FSI effect grows with increasing collision energies, however, even at the LHC energies it gives less then 5% increase of the charged hadron multiplicities and only small changes in the transverse momentum spectra. This PHSD finding is in line with the recent results by the Lund group [29] where the hadronic FSI effect has been incorporated in PYTHIA within a framework of the space-time picture of $p + p$ collisions. We also showed the influence on p_T spectra of the possible small QGP droplet formation in $p + p$ collisions at LHC energies and found only a very small effect here.

Finally, we stress the importance of the development of reliable event generators for elementary reactions from low to ultra-relativistic energies in view of heavy-ion physics.

Acknowledgements The authors acknowledge inspiring discussions and useful remarks from T. Sjöstrand and C. Bierlich. They are also grateful to C. Blume, W. Cassing, V. Lenivenko, P. Moreau, L. Oliva, K. Shtejer, O. Soloveva, T. Song and K. Werner for useful discussions and their interest to our work. We are grateful to S. Pulawski and M. Gazdzicki for providing us the experimental data from the NA61/SHINE Collaboration. Furthermore, we acknowledge support by the Deutsche Forschungsgemeinschaft (DFG, German Research Foundation): Grant BR 4000/7-1, by the Russian Science Foundation Grant 19-42-04101 and by the GSI-IN2P3 agreement under contract number 13-70. Also we thank the COST Action THOR, CA15213. We acknowledge funding from the European Union's Horizon 2020 research and innovation program STRONG-2020 under grant agreement No 824093. I.G. acknowledges support by the DFG through the Grant CRC-TR 211 'Strong-interaction matter under extreme conditions' – Project number 315477589 – TRR 211 and by HGS-HIRe for FAIR. The computational resources have been provided by the LOEWE-Center for Scientific Computing and the "Green Cube" at GSI.

Data Availability Statement This manuscript has no associated data or the data will not be deposited. [Authors' comment: This manuscript

is a theoretical study. There is no experimental data associated to this manuscript.]

References

1. B. Andersson, G. Gustafson, G. Ingelman, T. Sjostrand, Phys. Rep. **97**, 31 (1983)
2. B. Andersson, G. Gustafson, B. Soderberg, Z. Phys. C **20**, 317 (1983)
3. B. Nilsson-Almqvist, E. Stenlund, Comput. Phys. Commun. **43**, 387 (1987)
4. B. Andersson, G. Gustafson, H. Pi, Z. Phys. C **57**, 485 (1993)
5. T. Sjostrand, S. Mrenna, P.Z. Skands, JHEP **0605**, 026 (2006)
6. J. Schwinger, Phys. Rev. **83**, 664 (1951)
7. W. Cassing, E.L. Bratkovskaya, Phys. Rev. C **78**, 034919 (2008)
8. W. Cassing, Eur. Phys. J. ST **168**, 3 (2009)
9. W. Cassing, E.L. Bratkovskaya, Nucl. Phys. A **831**, 215 (2009)
10. E.L. Bratkovskaya, W. Cassing, V.P. Konchakovski, O. Linnyk, Nucl. Phys. A **856**, 162 (2011)
11. O. Linnyk, E.L. Bratkovskaya, W. Cassing, Prog. Part. Nucl. Phys. **87**, 50 (2016)
12. W. Cassing, E.L. Bratkovskaya, Phys. Rep. **308**, 65 (1999)
13. J. Aichelin, E. Bratkovskaya, A. Le Fèvre, V. Kireyeu, V. Kolesnikov, Y. Leifels, V. Voronyuk, G. Coci, Phys. Rev. C **101**, 044905 (2020)
14. S.A. Bass et al., Prog. Part. Nucl. Phys. **41**, 255 (1998)
15. M. Bleicher et al., J. Phys. G **25**, 1859 (1999)
16. O. Buss et al., Phys. Rep. **512**, 1 (2012)
17. J. Weil, V. Steinberg, J. Staudenmaier et al., Phys. Rev. C **94**, 054905 (2016)
18. K. Werner, F.M. Liu, T. Pierog, Phys. Rev. C **74**, 044902 (2006)
19. T. Pierog, I. Karpenko, J. Katzy, E. Yatsenko, K. Werner, Phys. Rev. C **92**, 034906 (2015)
20. S. Ostapchenko, Phys. Rev. D **83**, 014018 (2011)
21. G. Corcella, I. Knowles, G. Marchesini, S. Moretti, K. Odagiri, P. Richardson, M. Seymour, B. Webber, JHEP **01**, 010 (2001)
22. T. Sjöstrand, S. Ask, J.R. Christiansen, R. Corke, N. Desai, P. Ilten, S. Mrenna, S. Prestel, C.O. Rasmussen, P.Z. Skands, Comput. Phys. Commun. **191**, 159 (2015)
23. A. Peshier, W. Cassing, Phys. Rev. Lett. **94**, 172301 (2005)
24. W. Ehehalt, W. Cassing, Nucl. Phys. A **602**, 449 (1996)
25. N. Firdoua, Tuning of the PYTHIA 6.4 Multiple Parton Interaction model to Minimum Bias and Underlying Event data. CERN-THESIS-2013-419. 152 p. https://cds.cern.ch/search?ln=en&cc=CERN+Theses&sc=1&p=Firdoua&action_search=Search&op1=a&m1=a&p1=&f1=
26. W. Cassing, Nucl. Phys. A **700**, 618 (2002)
27. E. Seifert, W. Cassing, Phys. Rev. C **97**, 024913 (2018)
28. E. Seifert, W. Cassing, Phys. Rev. C **97**, 044907 (2018)
29. T. Sjöstrand, M. Utheim. arXiv:2005.05658 [hep-ph]
30. A. Casher, H. Neuberger, S. Nussinov, Phys. Rev. D **20**, 179 (1979)
31. B. Andersson, G. Gustafson, T. Sjöstrand, Z. Phys. C **6**, 235 (1980)
32. E.G. Gurvich, Phys. Lett. B **87**, 386 (1979)
33. G. Eichmann, H. Sanchis-Alepuz, R. Williams, R. Alkofer, C.S. Fischer, Prog. Part. Nucl. Phys. **91**, 1 (2016)
34. J. Geiss, W. Cassing, C. Greiner, Nucl. Phys. A **644**, 107 (1998)
35. E. Bratkovskaya, J. Aichelin, M. Thomere, S. Vogel, M. Bleicher, Phys. Rev. C **87**, 064907 (2013)
36. E.L. Bratkovskaya, W. Cassing, Nucl. Phys. A **807**, 214 (2008)
37. T. Song, H. Berrehrah, D. Cabrera, J.M. Torres-Rincon, L. Tolos, W. Cassing, E. Bratkovskaya, Phys. Rev. C **92**, 014910 (2015)
38. W. Cassing, L. Tolós, E.L. Bratkovskaya, A. Ramos, Nucl. Phys. A **727**, 59 (2003)
39. A. Ilner, D. Cabrera, C. Markert, E. Bratkovskaya, Phys. Rev. C **95**, 014903 (2017)
40. A. Ilner, J. Blair, D. Cabrera, C. Markert, E. Bratkovskaya, Phys. Rev. C **99**, 024914 (2019)
41. A. Ilner, J. Blair, D. Cabrera, C. Markert, E. Bratkovskaya, Phys. Rev. C **99**, 024914 (2019)
42. W. Cassing, A. Palmese, P. Moreau, E.L. Bratkovskaya, Phys. Rev. C **93**, 014902 (2016)
43. A. Palmese, W. Cassing, E. Seifert, T. Steinert, P. Moreau, E.L. Bratkovskaya, Phys. Rev. C **94**, 044912 (2016)
44. W. Cassing, K. Gallmeister, C. Greiner, Nucl. Phys. A **735**, 277 (2004)
45. N. Abgrall et al. (NA61/SHINE Collaboration), Eur. Phys. J. C **74**, 2794 (2014)
46. A. Aduszkiewicz et al. (NA61/SHINE Collaboration), Eur. Phys. J. C **77**, 617 (2017)
47. C. Alt et al. (NA49 Collaboration), Eur. Phys. J. C **45**, 343 (2006)
48. T. Anticic et al. (NA49 Collaboration), Eur. Phys. J. C **68**, 1 (2010)
49. T. Anticic et al. (NA49 Collaboration), Eur. Phys. J. C **65**, 9 (2010)
50. M. Gazdzicki, D. Röhrich, Z. Phys. C **71**, 55 (1996)
51. H. Schopper (ed.), *Landolt-Bornstein, NewSeries, Group I*, vol. 12 (Springer, Berlin, 1988)
52. M. Antinucci et al., Lett. Nuovo. Cimento Soc. Ital. Fis. **6**, 121 (1973)
53. A. Aduszkiewicz et al. (NA61/SHINE Collaboration). arXiv:2006.02062 [nucl-ex]
54. A. Aduszkiewicz et al. (NA61/SHINE Collaboration), Eur. Phys. J. C **76**, 198 (2016)
55. A. Aduszkiewicz et al. (NA61/SHINE Collaboration). arXiv:1912.10871 [hep-ex]
56. V. Friese et al. (NA49 Collaboration), J. Phys. G **30**, S119 (2004)
57. M.I. Gorenstein, M. Gazdzicki, K. Bugaev, Phys. Lett. B **567**, 175 (2003)
58. E. Bratkovskaya, S. Soff, H. Stoecker, M. van Leeuwen, W. Cassing, Phys. Rev. Lett. **92**, 032302 (2004)
59. B. Abelev et al. (STAR Collaboration), Phys. Rev. C **75**, 064901 (2007)
60. A. Adare et al. (PHENIX Collaboration), Phys. Rev. C **83**, 064903 (2011)
61. G. Alner et al. (UA5 Collaboration), Z. Phys. C **33**, 1 (1986)
62. C. Albajar et al. (UA1 Collaboration), Nucl. Phys. B **335**, 261 (1990)
63. B.B. Abelev et al. (ALICE Collaboration), Eur. Phys. J. C **73**, 2662 (2013)
64. J. Adam et al. (ALICE Collaboration), Eur. Phys. J. C **75**, 226 (2015)
65. A. Buckley, J. Butterworth, L. Lonnblad, D. Grellscheid, H. Hoeth, J. Monk, H. Schulz, F. Siegert, Comput. Phys. Commun. **184**, 2803 (2013)
66. M. Aaboud et al. (ATLAS Collaboration), Phys. Rev. C **96**, 024908 (2017)
67. E. Shuryak, I. Zahed, Phys. Rev. C **88**, 044915 (2013)
68. A. Bzdak, B. Schenke, P. Tribedy, R. Venugopalan, Phys. Rev. C **87**, 064906 (2013)
69. J. Adam et al. (ALICE), Nature Phys. **13**, 535 (2017)
70. C. Bierlich, G. Gustafson, L. Lönnblad, A. Tarasov, JHEP **03**, 148 (2015)